



**Post-staining Raman analysis of histological sections
following decolorization**

Journal:	<i>Analyst</i>
Manuscript ID	AN-ART-07-2022-001138
Article Type:	Paper
Date Submitted by the Author:	14-Jul-2022
Complete List of Authors:	<p>Akaji, Sakiko; Kyoto University, Department of Environmental Engineering, Graduate School of Engineering, Sagawa, Tomoya; Kyoto University, Graduate School of Global Environmental Studies; Kyoto Prefectural University of Medicine, Inflammation and immunology Honda, Akiko; Kyoto University, Graduate School of Global Environmental Studies; Kyoto University, Department of Environmental Engineering, Graduate School of Engineering Miyasaka, Natsuko; Kyoto University, Graduate School of Global Environmental Studies Sadakane, Kaori; Oita University of Nursing and Health Sciences Ichinose, Takamichi; Oita University of Nursing and Health Sciences Takano, Hirohisa; Kyoto University, Graduate School of Global Environmental Studies; Kyoto University, Department of Environmental Engineering, Graduate School of Engineering</p>

ARTICLE

Post-staining Raman analysis of histological sections following decolorization

Received 00th
January 20xx,

Sakiko Akaji,^a Tomoya Sagawa,^{b,c} Akiko Honda,^{a,c*} Natsuko Miyasaka,^c Kaori Sadakane,^d Takamichi Ichinose,^d Hirohisa Takano^{a,c}

Accepted 00th January 20xx

DOI: 10.1039/x0xx00000x

Hematoxylin and eosin (HE) staining of tissue sections is a powerful tool for observing changes in the tissue structure and is used as the most fundamental and vital technique in histology. However, xenobiotics such as polymers and inorganic or organic materials have low dyeability, making it difficult to observe the materials' distribution across tissues. Raman spectroscopy is an advantageous technique for identifying materials in tissue using spectroscopic fingerprints by laser irradiation without staining. In this study, we developed a combined method for morphological observation and Raman spectral acquisition on the identical tissue slide by employing a decolorization step to remove the eosin-induced fluorescence in HE-stained samples. Our method eliminated the fluorescence background and allowed the identical-field pathological observation, enabling simultaneous identification of biological responses and materials in the tissues.

Introduction

Tissue slides are an indispensable tool for observing detailed tissue structures by staining using dyes such as hematoxylin and eosin (HE). The HE staining technique provides useful information on the tissue definition and pathological structural changes in the tissue samples.

Recently, nanoparticles have been increasingly used in medicine and personal care products owing to their ultraviolet shielding, antioxidant, and biocidal properties¹. Some of these nanoparticles show xenobiotic characteristics, and their toxicity is unsuitable for the living organisms. Therefore, xenobiotics' influence on the living organisms and their underlying mechanisms is extensively studied; wherein, tissue slides are used as a critical element to clarify xenobiotics-induced pathological changes². It is important to analyze the localization of xenobiotics and the biological events that occur in their vicinity.

However, the HE staining technique alone is insufficient to identify the xenobiotics on the slide because of their low dyeability; therefore, other kinds of samples and/or techniques are utilized for their identification.

Raman spectroscopy is an effective technique in identifying materials using spectroscopic fingerprints by laser irradiation without staining them. Its application in the biological field has rapidly increased in recent times owing to its ability of cell or spectral tissue imaging. It identifies chemical substances and their distribution on a tissue slide, thereby helping in pathological research³. Raman spectroscopy can also show the chemical bond characteristics and distribution pattern of xenobiotics that helps understand the importance of xenobiotics distribution and its association with pathological, physiological and molecular biological changes as observed under histological examination, including HE and immunostaining.

The Raman signal is easily covered by the fluorescence signal because of its much stronger intensity. Raman scattering and fluorescence emission compete when the laser photons are absorbed by the fluorescence molecules including staining dyes. In addition, the laser irradiation can easily cause burn damages in the stained tissue slides. This feature limits Raman measurements in the stained tissue slides. To

^a Department of Environmental Engineering, Graduate School of Engineering, Kyoto University, Kyoto, Japan.

^b Inflammation and Immunology, Graduate School of Medical Science, Kyoto Prefectural University of Medicine, Kyoto, Japan.

^c Graduate School of Global Environmental Studies, Kyoto University, Kyoto, Japan.

^d Department of Health Science, Oita University of Nursing and Health Sciences, Oita 870-1201, Japan

† Footnotes relating to the title and/or authors should appear here.

Electronic Supplementary Information (ESI) available: [details of any supplementary information available should be included here]. See DOI: 10.1039/x0xx00000x

1
2
3 solve this problem, we subjected the tissue sections
4 initially to Raman spectroscopy prior to staining.
5 However, we faced a major challenge in locating an
6 appropriate measurement area, as it was hard to
7 distinguish the particles in the optical image captured
8 under Raman microscope. Previously, other various
9 techniques have been applied to avoid the fluorescence
10 background, such as changing the laser wavelength⁴ and
11 serial sections⁵. However, when we shifted to using
12 longer-wavelength excitation lasers lesser signal
13 intensity was observed. In addition, serial sections
14 occasionally do not show the same distribution because
15 their thickness changes the distribution of the tiny
16 materials.

17
18
19
20
21 In this study, we hypothesized that decolorization can
22 overcome the fluorescence background caused by the
23 dye. And the purpose of this study is to develop a novel
24 technique to observe HE-stained tissue structure with
25 implications in biological responses, and Raman
26 spectroscopic fingerprint distribution of xenobiotics on
27 an identical tissue slide. As a representative xenobiotic,
28 we employed titanium dioxide (TiO₂) particles because
29 they are easily detectable by Raman spectroscopy and
30 are widely used in various applications such as
31 cosmetics and paint; thus, TiO₂ exposure is prevalent
32 under general, occupational environment⁶. In this
33 study, we monitored the fluorescence features of the
34 dye, tested the influence of the decolorization step for
35 tissue structure and TiO₂ Raman signal, and confirmed
36 the tissue distribution of TiO₂.

43 44 Experimental

45 Fluorescence measurement

46
47 The HE-staining solution was measured using Duetta
48 fluorescence and absorbance spectrometer (HORIBA,
49 Kyoto, Japan). Samples were measured at room
50 temperature and diluted under 0.1 absorption in water
51 using a 1 cm fluorescence quartz cell. The absorbance-
52 transmittance and a fluorescence excitation-emission
53 matrix (A-TEEMs) were automatically corrected for the
54 influence of inner filter effects, and Rayleigh masking
55 was applied.

TiO₂ preparation

TiO₂ nanoparticles (Sakai Chemical Industry, Osaka, Japan) were dispersed in 10 mg/mL sterile phosphate-buffered saline (PBS) solution, sonicated, and used in animal experiments. The control mice received 100 μL PBS alone.

In the TiO₂ signal verification, the solution was dispersed in 0.005 mg/mL PBS and spread on a glass slide using cytospin (Cytospin 2; Shandon, Inc., Pittsburgh, PA, USA), centrifuged at 2000 rpm for 5 min. Subsequently, the slide was dried, paraffin-embedded, and stained with HE for signal verification.

Forming Tissue slide and decolorization

Male ICR mice (8 weeks old, n = 3 for TiO₂ exposure, N = 1 for control) were obtained from The Jackson Laboratory Japan (Yokohama, Japan) and housed in an animal facility for one week. They were fed a commercial diet (CE-2; CLEA Japan Inc., Tokyo, Japan), provided water *ad libitum*, and housed in an animal facility maintained at 22-25 °C with a 12:12 h light–dark cycle. All mice were treated humanely, and suffering was alleviated following the guidelines for animal experiments of the Oita university of Nursing and Health Sciences. All experiments, including animal experiments, were approved by the Animal Research Committee at Oita University of Nursing (approval number: 20-88, approval date: 26th March 2021).

After 24 h of intratracheal administration of 100 μL TiO₂ solution (50 μg/mouse), all mice were sacrificed and their lungs were fixed during inflation with 4% paraformaldehyde solution through a tracheal catheter, thereafter lungs were removed, embedded in paraffin, and sectioned at 5 μm thickness using a microtome.

For histological observation, the lung tissue sections derived from four different mice were stained with hematoxylin (S3301, DAKO, Agilent Technologies, Santa Clara, CA, USA) and eosin (051-06515, Wako, Osaka, Japan) and then enclosed using Marinol (20092, Muto Pure Chemicals, Tokyo, Japan). Stained tissue slides were observed using a BX-53 with a bright-field

condenser and an oil immersion dark-field condenser (Olympus, Tokyo, Japan), and a BZX-810 microscope (Keyence, Osaka, Japan).

After observing stained tissue sections, these slides were decolorized to remove artifacts for Raman measurement. First, the transparent cover glass slides were removed with xylene then hydrated using serial concentrations of ethanol, from 100% to 70%, before decolorization. In this step, slides were soaked for approximately 10–20 minutes at 80 and 70 % of ethanol to decolorize eosin. Next, the slides were soaked in the Target Retrieval Solution (S1699, DAKO), mainly consisting of citrate buffer pH 6, and heated in a microwave at 900 W for approximately 15 min at over 80 °C. Subsequently, slides were incubated overnight at 30 °C, washed after incubation using distilled water and then dehydrated using a series of solutions with ethanol and xylene concentrations.

Raman imaging and spectrum acquisition

Raman spectra and images were obtained using LabRAM HR Evolution confocal Raman microscope (HORIBA), using a LabRAM system employing a 532 nm excitation wavelength and a 100× objective lens (NA = 0.9) integrated with an Olympus microscope.

The decolorized samples were located on the piezoelectrically driven stage and then irradiated with an excitation laser of approximately 7 mW for the tissue section and 8 mW for TiO₂ particles. For Raman spectroscopic imaging, the acquisition step was set to 1 μm for 30 s at each point. For the TiO₂ Raman spectra measurements, the acquisition time was 5 s with 10 times integration. The acquired Raman spectra were preprocessed and analyzed using the Labspec6 software (HORIBA). For Raman imaging of tissue slides, the acquired spectra were processed using baseline collection, denoise spikes, and single value decomposition (SVD). Subsequently, the processed data were subjected to classical least squares (CLS) to determine TiO₂ and tissue distribution. For TiO₂, Raman spectra were preprocessed by baseline correction and normalization, and then the TiO₂ signal of each decolorizing step was compared.

Results

Fluorescence interference under 532 nm laser excitation for Raman measurement

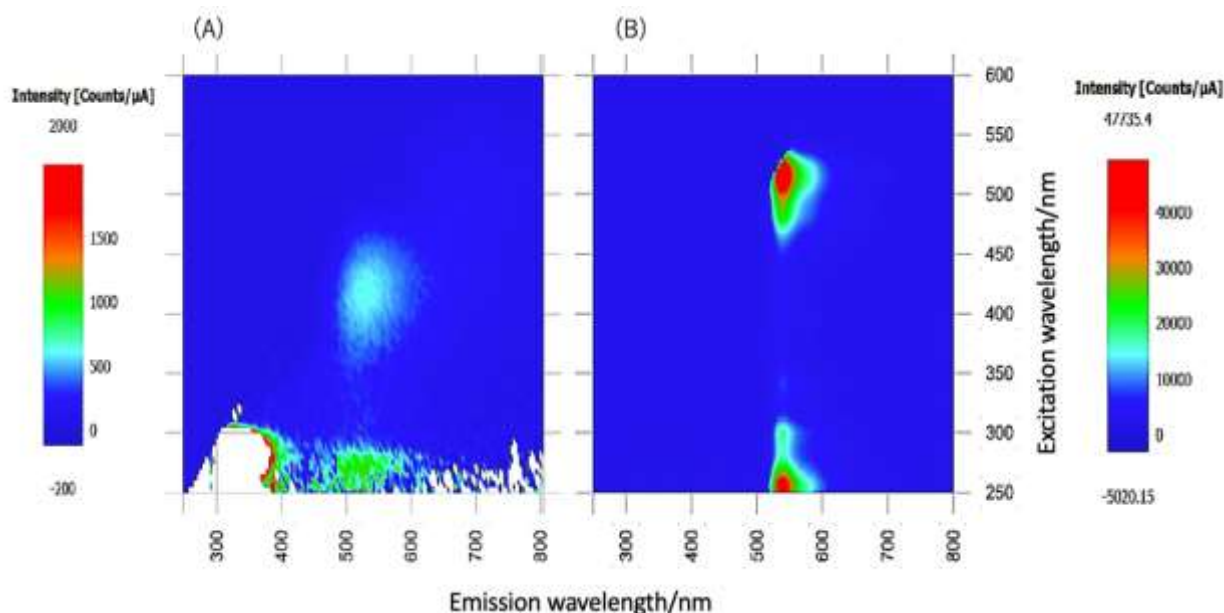


Figure 1. A-TEEM of hematoxylin (A) and eosin (B).

A-TEEM showed what excitation wavelength induce the emission of the dye. The pseudo color means the intensity counts of emission. A-TEEMs: The absorbance-transmittance and a fluorescence excitation-emission matrix

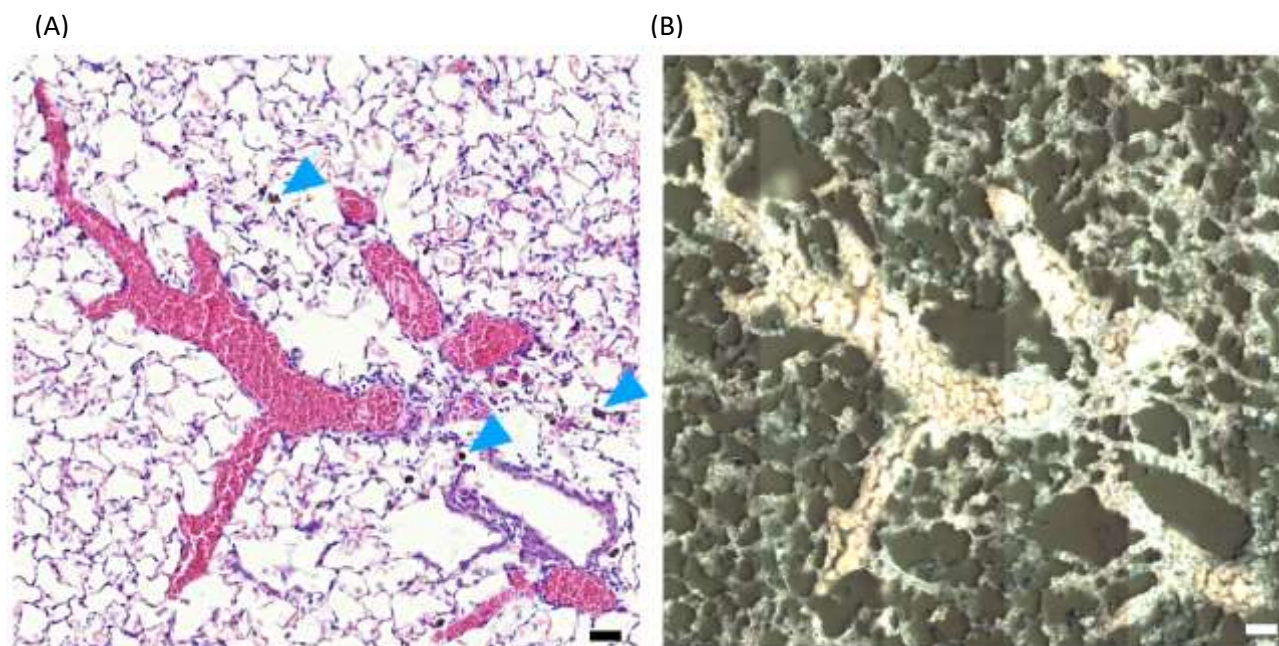


Figure 2. Representative images of mouse lung tissue sections after HE-staining (A) and decolorization in the same region (B). Bar = 50 μm . The lung tissue was obtained after 24h of TiO_2 intratracheal administration. (A) Blue arrowhead indicates TiO_2 location. TiO_2 : titanium dioxide, HE: hematoxylin and eosin

A 532 nm laser was used as the excitation wavelength for Raman detection. It is the most popular laser wavelength and provides a high wavenumber C-H region (2,800–3,000 cm^{-1}) in the same Raman capture wavelength window with a low wavenumber TiO_2 region (400–700 cm^{-1}). When we measured the Raman signal of a stained tissue slide using a 532 nm laser, there was no Raman signal due to the fluorescence interference. To clarify the fluorescence profile of the staining dye - HE, we obtained A-TEEM that is constructed using a 3D plot of the excitation or emission wavelength and intensity and the corrected its inner filter effect. Therefore, this matrix rapidly and accurately showed the fluorescence excitation and emission profile. The A-TEEM showed eosin dye having approximately 550 nm emission at 532 nm excitation (Figure 1), suggesting that eosin dye is emitted strongly when a Raman signal is obtained using 532 nm laser and must be removed to acquire Raman signals from the tissue slide.

The tissue structure and TiO_2 Raman spectra comparison before and after decolorization

To acquire the Raman signal by Raman spectroscopy from the same point as the HE-stained tissue slides, we

referred to the HE-stained tissue structure on the slide as it was difficult to localize TiO_2 distribution in the tissue slides after decolorization (Figure 2 (A)). To determine whether the tissue structure on the slides remained intact after the decolorization step, we compared the tissue structure before and after decolorization. We processed the tissue without dehydration, and the

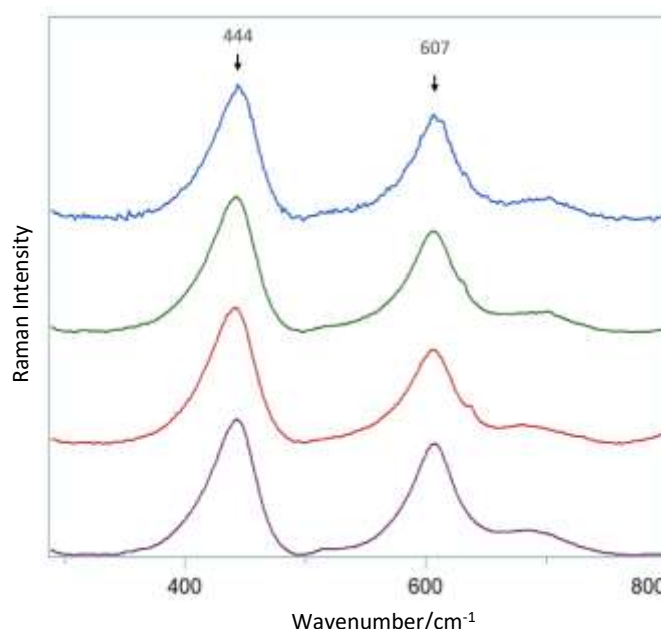


Figure 3. Comparison of TiO_2 spectrum during decolorization. The Raman spectra of TiO_2 after cover glass removal (blue), after eosin decolorizing (green), after hematoxylin decolorizing (red); only TiO_2 without any procedure (purple). TiO_2 : titanium dioxide

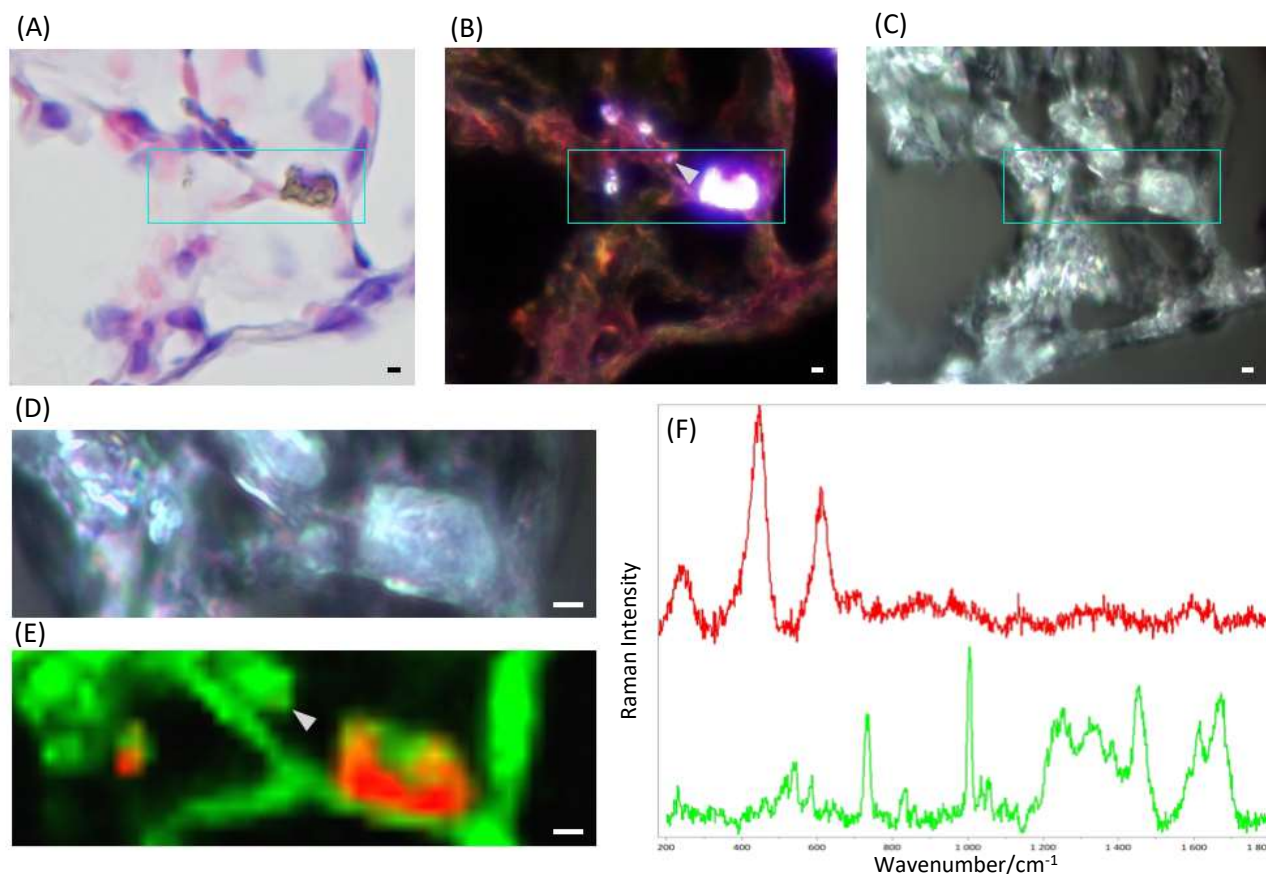


Figure 4. Representative data of Raman spectral imaging of decolorized tissue slide. The image of HE-stained tissue slide was taken by bright-field and dark-field microscopy. Then the identical tissue slide was decolorized and used for Raman spectral mapping, and the mapping data was applied for CLS processing. (A) HE-stained tissue image taken by bright-field microscopy. (B) HE-stained tissue image at the same point as A taken by dark-field microscopy. Gray arrowhead indicates where the particles were suspected to be present. (C) Decolorized tissue image at the same point as A. (D) Enlarged view of the blue square in C. (E) The CLS-processed image of the area viewed in D. Green area means a cell-derived signal; red area means TiO_2 -derived signal. Gray arrowhead indicates the same location as pointed in (B). (F) Spectra used for CLS processing. The red spectrum shows TiO_2 , and the green spectrum shows the cell-derived one. These spectra construct the CLS image shown in E. Bar = 2 μm , CLS: classical least squares, TiO_2 : titanium dioxide, HE: hematoxylin and eosin

decolorized tissue showed a distended structure compared with the HE-stained tissue (data not shown). With the addition of the dehydration step, the tissue structure returned to the shape as it was before decolorization (Figure 2 (B)).

The decolorization procedure had many more steps compared with unstained tissue slides, which are usually used for Raman measurement. Considering that this procedure damages the samples on slides, we investigated whether the decolorized material, TiO_2 , is damaged due to decolorization. The TiO_2 dispersed slides were treated by each dye or decolorization step, and TiO_2 Raman spectra were measured and compared. As a result, the TiO_2 spectrum from the decolorized step showed the same spectrum as before the procedure. In addition, the spectra during this procedure showed the same results (Figure 3), thereby suggesting that the

decolorization step has a minimal effect in optimal detection of TiO_2 Raman spectrum.

Raman imaging of decolorized tissue section

To confirm the accessibility of this decolorizing method for Raman analysis, we applied the procedure to mouse lung tissue exposed to TiO_2 nanoparticles. Upon observing HE-stained tissue slides using bright-field microscopy, TiO_2 appeared brown and localized within the cells (Figure 4(A)). The dark-field microscopic image also showed bright area which might suggest the existence of TiO_2 particles in the lung tissue (Figure 4(B)). The image after decolorization showed unclear TiO_2 localization under Raman microscopy without laser irradiation (Figure 4 (C), (D)). We then performed mapping measurements on decolorized slides under Raman microscopy. Due to decolorization, the autofluorescence of dyes became weak; hence the

acquired Raman spectra showed characteristic peaks of TiO₂ and cells without burn damage (Supplemental Figure 1). From the mapped spectrum, we found the TiO₂- and tissue-derived spectrum (Figure 4 (F)) and constructed a CLS-processed map image (Figure 4 (E)). The tissue-derived spectrum was obtained based on the Raman spectrum of PBS control tissue samples (Supplemental Figure 2). The CLS-constructed image clearly showed TiO₂ distribution in the tissue and the structure of decolorized tissue appeared similar to that observed in the HE-staining image. Similar results were obtained from different mice samples. Raman fingerprint mapping revealed the area that was initially suspected to be TiO₂ particle under dark-field microscopy (Figure 4 (B, arrowhead)) was not TiO₂ but a tissue.

Discussion

We developed a combined method for morphological observation and Raman spectral acquisition on the identical tissue slide by employing a decolorization step to remove the eosin-induced fluorescence in HE-stained samples. Our method eliminated the fluorescence background and allowed the identical-field pathological observation, enabling simultaneous identification of biological responses and materials in the tissues.

In particular, the difficulty of increasing nanoparticle spatial reproducibility in sequential tissue slides is because sequential tissue slides seldom do not show the same structure. This problem is due to the thickness of the tissue section and the small size of the target nanoparticles and cells. To date, the following techniques have been used to observe the distribution and identification of TiO₂: dark-field microscopy, electronic microscopy⁷, X-ray fluorescence microscopy⁸, fluorescence imaging⁹, and near-infrared (NIR) hyperspectral imaging¹⁰. Dark-field microscopy can easily obtain the image but cannot identify the detected particles. Electronic microscopy provides high-resolution images that clearly show organelles but cannot identify the detected particles. Although X-ray fluorescence microscopy is advantageous in comprehensively measuring the distribution of

nanoparticles and is non-destructive, the spatial resolution is insufficient for cell size observations. In the case of fluorescence microscopy, the fluorescence tags might yield conflicting results when comparing biological events because both TiO₂ and the fluorescence tags are xenobiotics. The NIR hyperspectral imaging non-invasively reveals TiO₂ distribution and can identify the material. However, the spectra typically show broad peaks that can be easily corrected by hydration. Compared with the above techniques, Raman microscopic measurement is convenient for identifying TiO₂ and other xenobiotics and their distribution when investigating biological events.

Material identification and clarifying the distribution of xenobiotics helps understand the morphological changes and biological events in tissues related to xenobiotics. Raman spectroscopy is rapidly emerging in the biological field because it can identify materials with minimal invasion without the need for labels^{11,12}. This feature makes it possible to apply Raman spectroscopy to living materials such as cells and tissues as well as inorganic or organic materials^{13, 14}. On the other hand, tissue slides treated with HE-staining or immunostaining have strong autofluorescence, which competes with Raman signals, leading to a major issue¹⁵. Therefore, Raman signal acquisition required a strategy to remove or mitigate background signals. However, each approach has shortcomings; for instance, acquiring Raman spectra before staining causes uncertainty regarding the appropriate target area; changing longer excitation laser wavelength can reduce the Raman signal intensity; using sequence tissue slides renders it difficult to maintain spatial reproducibility. To resolve the above major issues, we combined decolorization and Raman measurement of HE-stained tissue slides in this study. Ozawa et al. discussed decolorizing solutions such as phosphoric acid, carboxylic acid, and commercially available decolorizing solutions, which removed the chelation of hematoxylin¹⁶. The target retrieval solution, consisting of citric acid at pH 6, also showed the same decolorizing effect after heating. This hematoxylin decolorization strategy helps to conduct Raman measurements without the burn damage induced by

laser irradiation. Eosin, which has stronger fluorescence than hematoxylin at 532 nm excitation, is a water-soluble pigment; therefore, eosin seemed to be removed easily during hydration and decolorization steps¹⁶.

In the present study, both dark-field microscopic image and Raman fingerprint mapping image were applicable for the detection of xenobiotics, such as TiO₂, in the tissue sections. However, the result of Raman fingerprint mapping clearly showed that TiO₂ particles were not always localized in the area as speculated from the dark-field microscopic images. This result distinctly showed the advantage of Raman fingerprint mapping for identification of xenobiotics. On the other hand, extended Raman mapping takes long time, and the image taken by Raman microscopy without laser irradiation showed unclear location of xenobiotics. Based on these observations, we propose an efficient and effective method for xenobiotics detection in the tissue sections, wherein dark-field microscopy is first applied to screen the area where the xenobiotics are suspected, followed by Raman fingerprint mapping on the suspected area for the identification of xenobiotics.

Thus, this technique is applicable for Raman spectra acquisition in the identical HE-stained tissue slide under any excitation wavelength, which presents the relevance of preserving morphological structure, while simultaneously studying chemical fingerprint distribution of xenobiotics, furthermore providing means to re-use the valuable archived samples.

Conclusions

Our novel technique allows us to observe HE-stained structure and Raman fingerprint mapping on the identical tissue slide after a decolorizing step. This method helps in non-invasively identifying xenobiotics and their distribution and could be utilized for observing valuable slides such as pathological tissue sections. Furthermore, combining histological observation, such as HE and immunostaining, and Raman spectroscopy helps unraveling the relationships between xenobiotics distribution and pathological, physiological, and

molecular biological changes. Hence, this technique holds the potential to further develop the existing pathological examination methods.

Author Contributions

Sakiko Akaji: Data curation, Formal analysis, Methodology, Investigation, Visualization, Writing - Original Draft, **Tomoya Sagawa:** Conceptualization, Formal Analysis, Investigation, Methodology, Writing - Review & Editing, **Akiko Honda:** Project administration, Resources, Writing - Review & Editing, **Natsuko Miyasaka:** Formal analysis, Investigation, Methodology, Visualization, Writing - Review & Editing, **Kaori Sadakane:** Investigation, Writing - Review & Editing, **Takamichi Ichinose:** Investigation, Writing - Review & Editing, **Hirohisa Takano:** Conceptualization, Supervision, Funding acquisition, Writing - Review & Editing

Conflicts of interest

There are no conflicts to declare.

Acknowledgements

The authors thank M. Tanaka and R. Ohata (Graduate School of Global Environmental Studies, Kyoto University, Kyoto, Japan) for experimental assistance. The current affiliation of T. Ichinose is Graduate School of Global Environmental Studies, Kyoto University, Kyoto. This work was supported by the Core Research for Evolutional Science and Technology (CREST) program of the Japan Science and Technology Agency (JST), Japan [grant number JPMJCR19H3].

Notes and references

- 1 V. Montesinos-Cruz, J. Rose, A. Pappa, M. I. Panayiotidis, A. D. Vizcaya-Ruiz, R. Franco, *Chem. Res. Toxicol.*, 2020; **33**, 536-552
- 2 R. Cornu, A. Meduneau, H. Martin, *Toxicology*, 2020; **430**, 152344
- 3 C. Krafft, M. Schmitt, I. W. Schie, D. Cialla-May, C. Matthaus, T. Bocklitz, J. Popp, *Angew. Chem. Int. Ed.*, 2017; **56**, 4392-4430
- 4 L. Machtoub, R. Pfeiffer, A. Backovic, S. Frischauf, M. C. Wick, *J Med Imaging Radiat Sci.*, 2010; **41**, 159-164
- 5 T. H. Tsai, M. A. Short, D. I. McLean, H. Zeng, K. McElwee, H. Lui, *Analyst*, 2014; **139**, 2799

ARTICLE

Journal Name

- 6 K. Schilling, B. Brandoed, D. Castelli, E. Dufour, J. F. Nash, W. Pape, S. Schulte, I. Tooley, J. van den Bosch, F. Schellauf, *Photochem. Photobiol. Sci.*, 2010; **9**, 495-509
- 7 P. H. Danielsen, K. B. Kundsén, J. Strancar, P. Umerk, T. Koklic, M. Gravas, E. Vanhala, S. Savukoski, Y. Ding, A. M. Madsen, N. R. Jacobsen, I. K. Weydahl, T. Berthing, S. S. Poulsen, O. Schmid, H. Wolff, U. Vogel, *Toxicol. Appl. Pharmacol.*, 2020; **386**, 114830
- 8 G. Zhang, N. Shinohara, H. Kano, H. Senoh, M. Suzuki, T. Sasaki, S. Fukushima, M.gamo, *J. Appl. Toxicol.*, 2016; **36**, 1268-1275
- 9 G. Xie, C. Wang, J. Sun, G. Zhong, *Toxicology Letters*, 2015; **205**, 55-61
- 10 M. Husain, A. T. Saber, C. Guo, N. R. Jacobsen, K. A. Jensen, C. L. Yauk, A. Williams, U. Vogel, H. Wallin, S. Halappanavar, *Toxicol. Appl. Pharmacol.*, 2013; **269**, 250-262
- 11 L.Ou, A. Honda, N. Miyasaka, S. Akaji, I. Omori, R. Ishikawa, K. Ueda, H. Takano, *Toxicol. Mech. Methods*, 2021, DOI: 10.1080/15376516.2021.2008569.
- 12 T. Sagawa, A. Honda, R. Ishikawa, N. Miyasaka, M. Nagao, S. Aakaji, T. Kida, T. Tsujikawa, T. Yoshida, Y. Kawahito, H. Takano, *Nanotoxicology*, 2021, DOI: 10.1080/17435390.2021.2022231.
- 13 B. Kann, H. L. Offerhaus, M. Windbergs, C. Otto, *Adv. Drug. Deliv. Rev.*, 2015; **89**, 71-90
- 14 M. Okuda, N. I. Smith, A. F. Palonpon, H. Endo, S. Kawata, M. Sodeoka, K. Fujita, *PNAS*, 2012; **109**, 28-32
- 15 L. Mavarani, D. Petersen, S. F. El-Mashtoly, A. Mosig, A. Tannapfel, C. Kottling, K. Gerrwert, *Analyst*, 2013; **138**, 4035-4039
- 16 A. Ozawa, M. Sakaue, *Annals of Anatomy*, 2020; **227**, 151431